

Displacement-Sparse Neural Optimal Transport

Peter Chen^{1,2} Yue Xie² Qingpeng Zhang^{2,3}

Abstract

Optimal Transport (OT) theory seeks to determine the map $T : X \rightarrow Y$ that transports a source measure P to a target measure Q , minimizing the cost $c(\mathbf{x}, T(\mathbf{x}))$ between \mathbf{x} and its image $T(\mathbf{x})$. Building upon the Input Convex Neural Network OT solver (Makkuva et al., 2020; Amos et al., 2017) and incorporating the concept of displacement-sparse maps (Cuturi et al., 2023), we introduce a sparsity penalty into the minimax Wasserstein formulation, promote sparsity in displacement vectors $\Delta(\mathbf{x}) := T(\mathbf{x}) - \mathbf{x}$, and enhance the interpretability of the resulting map. However, increasing sparsity often reduces feasibility, causing $T_{\#}(P)$ to deviate more significantly from the target measure. In low-dimensional settings, we propose a heuristic framework to balance the trade-off between sparsity and feasibility by dynamically adjusting the sparsity intensity parameter during training. For high-dimensional settings, we directly constrain the dimensionality of displacement vectors by enforcing $\dim(\Delta(\mathbf{x})) \leq l$, where $l < d$ for $X \subseteq \mathbb{R}^d$. Among maps satisfying this constraint, we aim to identify the most feasible one. This goal can be effectively achieved by adapting our low-dimensional heuristic framework without resorting to dimensionality reduction. We validate our method on both synthesized sc-RNA and real 4i cell perturbation datasets, demonstrating improvements over existing methods.

1. Introduction

Optimal transport (OT) aims to find a map T that efficiently transfers mass from one measure to another under the ground-truth cost. This technique has been applied in various machine-learning-based single-cell biology studies,

¹Department of Mathematics, Columbia University, New York, USA ²HKU Musketeers Foundation Institute of Data Science, Hong Kong ³HKU Shanghai Intelligent Computing Research Center, Shanghai, China. Correspondence to: Yue Xie <yxie@hku.hk>, Qingpeng Zhang <qpzhang@hku.hk>.

as demonstrated in (Huizing et al., 2022; Zhang et al., 2021; Demetci et al., 2022; Schiebinger et al., 2019; Bunne et al., 2023b). Compared to traditional methods of solving OT, such as Sinkhorn's algorithm (Cuturi, 2013), recent studies in single-cell biology have increasingly utilized Neural Optimal Transport (Neural OT) solvers. These solvers efficiently scale OT to large-scale and high-dimensional problems using continuous methods (Korotin et al., 2021b). For instance, CellOT (Bunne et al., 2023b) addresses cell perturbation response by leveraging Neural OT, implemented via the Input Convex Neural Network (ICNN) framework.

While Neural OT solvers can produce feasible maps, the lack of sparsity in the displacement vector reduces their interpretability, often resulting in overly complex OT maps that involve all dimensions (features). To address the similar issue in the Sinkhorn-solved map, Cuturi et al. (2023) introduced the concept of displacement-sparse maps. These maps are more interpretable with lower-dimensional displacement while preserving their applicability in the original space without relying on dimensionality reduction techniques. Inspired by this work, we extend similar sparsity-promoting features to Neural OT solvers, specifically the Neural OT solver implemented via ICNN (Makkuva et al., 2020) (referred to as “ICNN OT” in the following discussion).

Building on the minimax formulation of the Kantorovich dual problem used in ICNN OT, we incorporate sparsity penalties into the framework. This builds on the re-parameterization of the dual potentials f and g as convex functions, which can be efficiently learned through ICNN training. The sparsity penalty is inspired by the Cuturi et al. (2023)’s sparsity-induced transportation cost function, which is defined as $c(\mathbf{x}, \mathbf{y}) = \frac{1}{2} \|\mathbf{x} - \mathbf{y}\|_2^2 + \lambda \cdot \tau$. Here, τ serves as a sparsity regulator, and λ controls the intensity of the sparsity-inducing.

However, inducing sparsity in OT maps comes with a trade-off: as the sparsity level increases, the accuracy of the map’s feasibility decreases, which means that the source measure cannot be effectively transported to the target measure. This effect is evident in Figure 2, where at higher sparsity intensity level, less points can be effectively transported to the target location, and displacement vectors are becoming shorter due to the stronger sparsity penalty. To tackle this

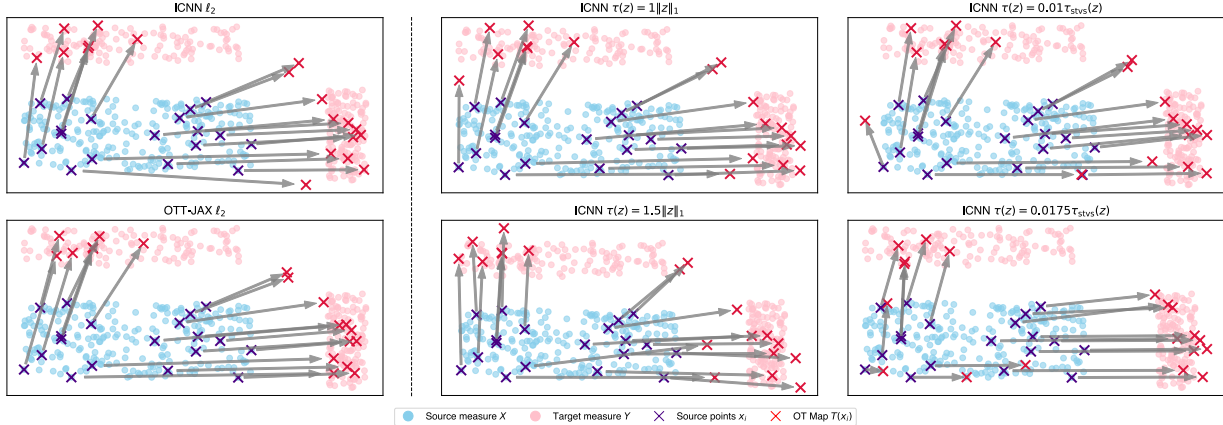


Figure 1. OT maps induced by various sparsity penalties $\tau(\cdot)$ at different intensity levels λ . The first column presents the maps produced by ICNN OT and the traditional Sinkhorn algorithm implemented using OTT-JAX (Cuturi et al., 2022), both without sparsity penalties. The subsequent columns illustrate maps learned via ICNN with sparsity penalties, specifically ℓ_1 and τ_{stvs} : the top row corresponds to maps trained with lower sparsity intensities, while the bottom row represents maps trained with higher sparsity intensities. Randomly selected points from the source distribution are used to showcase the displacement vectors (arrows) learned through OT. Example of aggregate results are shown in Figure 2.

issue, we create a dynamic framework to adjust the sparsity intensity, offering two models to solve OT tasks in both low-dimensional and high-dimensional spaces.

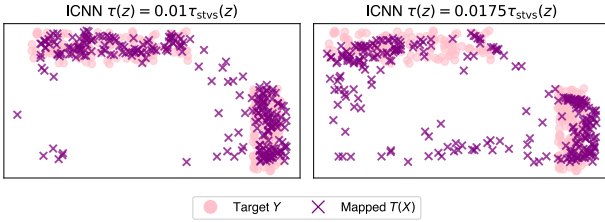


Figure 2. Aggregate results for τ_{stvs} at different sparsity intensity levels. A comparison between the mapped source elements $T(X)$ and the target elements Y is shown.

Contributions. We introduce an intuitive method to incorporate sparsity penalties into the loss function to solve the biased OT map, while providing theoretical guarantees. Different from the Sinkhorn OT solver, where sparsity intensity cannot be dynamically adjusted, our framework leverages ICNN to enable a novel approach for dynamically controlling sparsity intensity:

- We embed sparsity penalty functions into the ICNN OT framework. For low-dimensional spaces, we utilize two sparsity penalties summarized in Cuturi et al. (2023): the ℓ_1 -norm and τ_{stvs} . For high-dimensional spaces, we introduce a novel smoothed ℓ_0 -norm (Mohimani et al., 2007) as the sparsity penalty.
- For low-dimensional tasks, we propose a novel framework within the ICNN training process that dynamically adjusts the sparsity intensity λ . This allows users

to effectively balance the trade-off between the feasibility of the map and the level of induced sparsity. For high-dimensional tasks, instead of using two metrics, we constrain the dimensionality of displacement vectors directly, seeking the most feasible map within these constraints. This is achieved by adapting the heuristic framework developed for low-dimensional tasks.

2. Related Works

Neural Optimal Transport. Neural OT solvers employ continuous methods to estimate transportation plans or dual potentials through neural networks, avoiding the discrete formulations typically used by traditional approaches. Popular methods (Taghvaei & Jalali, 2019; Makkula et al., 2020; Fan et al., 2021; Korotin et al., 2021a; Mokrov et al., 2021; Bunne et al., 2022; Alvarez-Melis et al., 2022) often reparameterize the transportation plan or dual potentials and leverage ICNN (Amos et al., 2017) for approximation. In addition, Korotin et al. (2021b) provides a benchmark for evaluating the performance of current neural OT solvers, and Asadulaev et al. (2024) proposes a framework to solve neural OT problems with general cost functions.

In line with CellOT (Bunne et al., 2023b), we utilize the minimax formulation of dual potentials from Makkula et al. (2020) to introduce displacement sparsity. Comparing to other neural OT solvers, this formulation was chosen because it provides a straightforward approach to recovering displacement vectors through dual potentials.

Unlike Sinkhorn OT solvers, which relies on entropic reg-

ularization and fixed cost functions, neural OT solvers can dynamically learn transport maps for unfixed measures and generalize across tasks with dynamic loss functions. This ability to adapt makes neural OT solvers highly versatile in a variety of optimal transport applications. It is also worth clarifying that approaches based on the Wasserstein Generative Adversarial Network (W-GAN) (Arjovsky et al., 2017; Gulrajani et al., 2017; Wei et al., 2018) do not compute OT mappings or transportation plans directly; rather, they use the Wasserstein distance as a loss function during training.

Displacement-sparse Optimal Transport. Cuturi et al. (2023) laid the groundwork for incorporating sparsity into displacement vectors in OT by formulating a framework using proximal operators of the sparsity penalty τ in the elastic cost to recover the OT map T . Building on this, Klein et al. (2024) proposed a framework to recover the OT map under any elastic cost without relying on proximal operators. Under the framework of neural OT, our work generalizes the formulation to allow the use of any sparsity penalties, even when their proximal operators are not well-defined.

Sparsity-related Optimal Transport. Apart from displacement sparsity, other works have explored different aspects of sparsity in the context of OT. Liu et al. (2023) introduced a regularization method to control the column cardinality of the transportation plan matrix, enhancing both storage efficiency and computational complexity. Similarly, Blondel et al. (2018) proposed a regularization approach using the ℓ_2^2 -norm to address the dense and complex transportation plans typically produced by the entropic-regularized Sinkhorn solution.

3. Preliminaries

3.1. Optimal Transport

Given two probability measure P and Q in \mathbb{R}^d and quadratic transportation cost, the Monge (1781) problem seeks to find the transport map $T : \mathbb{R}^d \rightarrow \mathbb{R}^d$ that minimizes the transportation cost:

$$T^* = \arg \min_{T: T_\# P = Q} \frac{1}{2} \mathbb{E}_{X \sim P} \|T(X) - X\|^2. \quad (1)$$

Here, T^* is the optimal transport map among all maps T that push forward P to Q . However, solving (1) is challenging because the set of feasible maps T may not be convex or might not exist at all. To address this, Kantorovich relaxed the problem by allowing mass splitting, replacing the direct map T with a coupling π between P and Q :

$$W_2^2(P, Q) = \inf_{\pi \in \Pi(P, Q)} \frac{1}{2} \mathbb{E}_{(X, Y) \sim \pi} \|X - Y\|^2, \quad (2)$$

where $\Pi(P, Q)$ is the set of all couplings (or transport plans) between P and Q . This relaxation makes the problem con-

vex and solvable via linear programming, with the optimal value being the squared 2-Wasserstein distance. To recover the map T from a coupling Π , one can use Kantorovich's dual formulation (Villani, 2003):

$$W_2^2(P, Q) = \sup_{(f, g) \in \Phi_c} (\mathbb{E}_P[f(X)] + \mathbb{E}_Q[g(Y)]), \quad (3)$$

$\Phi_c = \{(f, g) \in L^1(P) \times L^1(Q) : f(x) + g(y) \leq c(x, y)\}$ is the constraint space for the dual potentials f and g , with $L^1(P)$ denoting the set of integrable functions with respect to P , defined as $\{f : f \text{ is measurable and } \int |f| dP < \infty\}$, and $c(x, y)$ represents the transportation cost. Given the quadratic cost $c(x, y) = \frac{1}{2} \|x - y\|_2^2$ and under the saturated condition $f(x) + g(y) = \frac{1}{2} \|x - y\|_2^2$, map T from Q to P can be recovered via $y - \nabla f^*(y)$ (Brenier, 1991), where $f^*(y) = \sup_{x \in \mathbb{R}^n} (\langle x, y \rangle - f(x))$ denotes the convex conjugate of $f(y)$.

The dual potentials in the constraint of (3) can be further reparameterized as functions in convex space. Note that this reparameterization can only be performed under the quadratic cost function, implying that Cuturi et al. (2023)'s sparsity-regularized cost cannot be applied here. Eventually, (3) can be reformulated into the following minimax formulation (Makkuva et al., 2020, Theorem 3.3):

$$W_2^2(P, Q) = \sup_{\substack{f \in \text{CVX}(P) \\ f^* \in L^1(Q)}} \inf_{g \in \text{CVX}(Q)} \mathcal{V}_{P, Q}(f, g) + C_{P, Q}, \quad (4)$$

where $\mathcal{V}_{P, Q}(f, g) = -\mathbb{E}_P[f(X)] - \mathbb{E}_Q[\langle Y, \nabla g(Y) \rangle - f(\nabla g(Y))]$, $C_{P, Q} = \frac{1}{2} \mathbb{E}[\|X\|^2 + \|Y\|^2]$ is a constant, and $\text{CVX}(P)$ denotes the set of all convex functions in $L^1(P)$. The new minimax formulation parameterizes f and g into the convex space using a separate alternating optimization scheme, which can be learned via ICNN.

3.2. Input Convex Neural Network

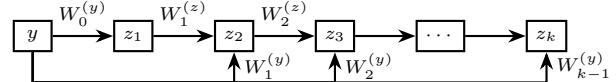


Figure 3. Input Convex Neural Network (ICNN) Structure.

Amos et al. (2017) introduced Input Convex Neural Networks (ICNNs) to model convex functions by optimizing a set of parameters, $\{W_i^{(y)}, W_i^{(z)}\}$, during each iteration.

Given an initial input y , the ICNN learns the convex function z_k through the following formulation:

$$z_{i+1} = g_i \left(W_i^{(z)} z_i + W_i^{(y)} y + b_i \right), \quad f(y; \theta) = z_k,$$

where z_i represents the layer activations, $\theta = \{W_{0:k-1}^{(y)}, W_{1:k-1}^{(z)}, b_{0:k-1}\}$ denotes the model parameters

($W_{0:k-1}^{(y)}$ and $W_{1:k-1}^{(z)}$ are weight matrices, and $b_{0:k-1}$ are bias terms), and g_i is a non-linear activation function. During each iteration, a small batch is drawn from both the source and target domains, and the ICNN learns f and g within $\text{ICNN}(\mathbb{R}^d)$ by optimizing the minimax problem with parameters θ_f and θ_g .

To ensure the convexity of the network, weights $W_i^{(y)}$ and $W_i^{(z)}$ must remain non-negative. [Makkuva et al. \(2020\)](#) demonstrated the feasibility of adding an arbitrary bounds to θ during the training process; This implementation indicates that θ_f and θ_g can be learned from a compact and uniformly bounded function space $\text{ICNN}(\mathbb{R}^d)$ given $P, Q \in \mathbb{R}^d$, which could simplify the original convex function space by restricting it to a smaller subspace compatible with $\text{ICNN}(\mathbb{R}^d)$:

Assumption 3.1. We assume that both source measure P and target measure Q admits a density with respect to the Lebesgue measure, and that there exist convex subsets $\mathcal{S}(P) \subset \text{CVX}(P)$ and $\mathcal{S}(Q) \subset \text{CVX}(Q)$ which are uniformly bounded. During the ICNN training, we have $\text{ICNN}(\mathbb{R}^d) \subset \mathcal{S}(P)$ and $\text{ICNN}(\mathbb{R}^d) \subset \mathcal{S}(Q)$.

Proposition 3.2. *Under Assumption 3.1, there exists an optimal solution (f_0, g_0) . Furthermore, the corresponding optimal transport map T from Q to P can be directly recovered via ∇g_0 .*

3.3. Sparsity-inducing Penalties τ

[Cuturi et al. \(2023\)](#) proposed the following cost function to induce displacement sparsity:

$$c(\mathbf{x}, \mathbf{y}) = \frac{1}{2} \|\mathbf{x} - \mathbf{y}\|_2^2 + \lambda \cdot \tau(\mathbf{y} - \mathbf{x}). \quad (5)$$

Under this regularized cost, the optimal transport mapping can be expressed as:

$$T(\mathbf{x}) = \mathbf{x} - \text{prox}_\tau \left(\mathbf{x} - \sum_{j=1}^m p^j(\mathbf{x}) (\mathbf{y}^j + \nabla \tau(\mathbf{x} - \mathbf{y}^j)) \right),$$

where prox_τ denotes the proximal operator of τ , and $p^j(\mathbf{x})$ represents the \mathbf{x} -dependent Gibbs distribution over the m -simplex. [Cuturi et al. \(2023\)](#) introduced three choices for the penalty function τ : the ℓ_1 -norm, Vanishing Shrinkage STVS (τ_{stvs}), and k -overlap norm ([Argyriou et al., 2012](#)). However, the k -overlap was ultimately abandoned due to its undesirable computational cost.

ℓ_1 -Norm. The ℓ_1 -norm directly penalizes the magnitude of the displacement vector, encouraging it to move towards the nearest target and inducing sparsity.

Vanishing Shrinkage STVS. [Schreck et al. \(2015\)](#) introduce the soft-thresholding operator with vanishing shrink-

age (STVS) for displacement vector \mathbf{z} ,

$$\tau_{\text{stvs}}(\mathbf{z}) = \gamma^2 \mathbf{1}_d^T \left(\sigma(\mathbf{z}) + \frac{1}{2} - \frac{1}{2} e^{-2\sigma(\mathbf{z})} \right),$$

where $\sigma(\mathbf{z}) = \text{asinh}(\frac{\mathbf{z}}{2\gamma})$ with element-wise operations.

However, both the ℓ_1 -norm and τ_{stvs} fail to directly reflect the dimensionality of the displacement vector. To address this, we introduce the most straightforward dimensionality penalty, the ℓ_0 -norm, into our model. Empirically, we find that a smoothed version of the ℓ_0 -norm is more suitable for the gradient descent scheme in ICNN training.

Smoothed ℓ_0 -Norm. To approximate the discontinuous ℓ_0 -norm, [Mohimani et al. \(2007\)](#) proposed replacing the indicator function $\nu(\mathbf{z})$, where $\nu(\mathbf{z}) = 1$ if $\mathbf{z} \neq 0$ and $\nu(\mathbf{z}) = 0$ otherwise, with a smooth Gaussian function:

$$f_\sigma(\mathbf{z}) = \exp \left(-\frac{\mathbf{z}^2}{2\sigma^2} \right).$$

As $\sigma \rightarrow 0$, $f_\sigma(\mathbf{z})$ approximates $1 - \nu(\mathbf{z})$. The smoothed ℓ_0 -norm is thus given by $n - \sum_{i=1}^n f_\sigma(\mathbf{z}_i)$. Note that the smoothed ℓ_0 -norm is non-convex, meaning its proximal operator may not be well defined and therefore cannot be directly applied to (5) to recover the mapping T .

4. Sparsity-inducing Minimax Formulation

Our goal is to bring sparsity to the displacement vector $\Delta(\mathbf{x}) := T(\mathbf{x}) - \mathbf{x}$ from the map T learned via ICNN, making the result with better interpretability. We introduce the sparsity penalty to the minimax formulation (4), which makes the squared 2-Wasserstein biased:

$$\widetilde{W}_2^2(P, Q) = C_{P,Q} + \sup_{f \in \mathcal{S}(P)} \inf_{g \in \mathcal{S}(Q)} \mathcal{V}_{P,Q}(f, g) + \lambda \int_{\mathbb{R}^d} \tau(\nabla g(y) - y) dQ, \quad (6)$$

where $\nabla g(y) - y$ represents displacement vector derived from (4), and λ is a parameter that controls the intensity of sparsity-inducing.

As discussed in §3.1, it is infeasible to re-parameterize the dual potentials into (4) when the quadratic cost is not used. Therefore, we adopt an intuitive approach to penalize the map as a whole. In this formulation, any τ function can be applied to recover the mapping without relying on prox_τ . Leveraging ICNN, we propose a heuristic framework in §4.1 that dynamically adjusts the intensity λ based on different goals, a feature not applicable to traditional Sinkhorn solvers. Several theoretical guarantees are introduced:

Lemma 4.1. *Let τ be the sparsity penalty introduced in §3.3. Assume that P and Q are probability measures*

over \mathbb{R}^d with bounded support. Moreover, suppose that $\mathcal{S}(P)$ and $\mathcal{S}(Q)$ contains only L -Lipschitz continuous functions f and g respectively. Then, the sparsity penalty $\int_{\mathbb{R}^d} \tau(\nabla g(y) - y) dQ$ is bounded for any $g \in \mathcal{S}(Q)$.

Remark 4.1. The bounded support assumption for Q in Lemma 4.1 is reasonable, as it is feasible to impose arbitrary bounds on the parameters within the $\text{ICNN}(\mathbb{R}^d)$ training space, proposed by Makkula et al. (2020, Remark 3.4). This assumption holds for the rest theoretical results in §4.

Theorem 4.2. Let J_0 denote the Wasserstein distance as defined in equation (4), and let J_λ denote the biased Wasserstein distance as defined in equation (6). Then, we have:

$$\lim_{\lambda \rightarrow 0} J_\lambda = J_0.$$

Theorem 4.3. Let $\mathcal{G} \subseteq \mathcal{S}(Q) \times \mathcal{S}(P)$ be the closed set of optimal solutions (g_0, f_0) to the optimization problem in (4), and let (g_λ, f_λ) be an optimal solution of (6), for a given $\lambda \geq 0$ and a convex regularizer τ , we have

$$\lim_{\lambda \rightarrow 0} \text{dist}((g_\lambda, f_\lambda), \mathcal{G}) = 0,$$

where $\text{dist}((g, f), \mathcal{G}) = \inf_{(g_0, f_0) \in \mathcal{G}} \| (g, f) - (g_0, f_0) \|$ denotes the distance from the point (g, f) to the set \mathcal{G} in an appropriate normed space.

Note that (g_λ, f_λ) converges to a unique (g_0, f_0) only if the objective function is strongly concave-strongly convex.

Theorem 4.4. Let $(g_{\lambda_1}, f_{\lambda_1})$ and $(g_{\lambda_2}, f_{\lambda_2})$ be the optimal solutions to the optimization problem defined in equation (6) for $\lambda = \lambda_1$ and $\lambda = \lambda_2$, respectively, where $0 \leq \lambda_1 < \lambda_2$, and let τ be a convex regulator. Then, the following inequality holds:

$$\int_{\mathbb{R}^d} \tau(\nabla g_{\lambda_1}(y) - y) dQ \geq \int_{\mathbb{R}^d} \tau(\nabla g_{\lambda_2}(y) - y) dQ.$$

Theorem 4.2 establishes that the formulation remains unbiased in the limit as $\lambda \rightarrow 0$. Theorem 4.3 demonstrates the convergence of the dual potentials specifically for convex regulators. Theorem 4.4 shows the monotonicity of the map's sparsity level as λ increases. However, we empirically observe that our non-convex regulators also exhibit these properties, as discussed in a later section. Proofs of these theorems and Lemma 4.1 are provided in Appendix A. The proofs proceed by first establishing Lemma A.2, which, combined with von Neumann (1928)'s Minimax Theorem, are used to prove the rest of the theorems. Examples of mappings learned with different τ penalties and a constant λ are shown in Figure 1.

To align with ICNN training, we restrict our training space

in (6) from $\mathcal{S}(P)$ and $\mathcal{S}(Q)$ to its subspace $\text{ICNN}(\mathbb{R}^d)$:

$$\begin{aligned} \widetilde{W}_2^2(P, Q) = C_{P,Q} + & \sup_{f \in \text{ICNN}(\mathbb{R}^d)} \inf_{g \in \text{ICNN}(\mathbb{R}^d)} \mathcal{V}_{P,Q}(f, g) \\ & + \lambda \int_{\mathbb{R}^d} \tau(\nabla g(y) - y) dQ, \end{aligned} \quad (7)$$

We also establish a bound on the deviation of the optimal transport map ∇g_λ in (6). For brevity, define

$$\mathcal{N}_{P,Q}(f, g) = \mathcal{V}_{P,Q}(f, g) + \lambda \int_{\mathbb{R}^d} \tau(\nabla g(y) - y) dQ,$$

Let (g_λ, f_λ) denote the optimal solution to the minimax problem (6). For any pair (g, f) , the minimization gap ϵ_1 and maximization gap ϵ_2 are defined as follows:

$$\epsilon_1(f, g) = \mathcal{N}_{P,Q}(f, g) - \inf_{g' \in \mathcal{S}(Q)} \mathcal{N}_{P,Q}(f, g') \geq 0,$$

$$\epsilon_2(f) = \mathcal{N}_{P,Q}(f_\lambda, g_\lambda) - \inf_{g' \in \mathcal{S}(Q)} \mathcal{N}_{P,Q}(f, g') \geq 0.$$

From Lemma 4.1, the penalty term $\tau(\nabla g(y) - y)$ is bounded. For simplicity, let $s(g) = \int_{\mathbb{R}^d} \tau(\nabla g(y) - y) dQ$, where $s(g)$ is bounded between 0 and M_τ , with M_τ being a constant depending on τ (details provided in Appendix A). Consequently, the sparsity gap between any two functions g_i and g_j , given by $\|s(g_i) - s(g_j)\|$, is also bounded by M_τ . With the definitions of ϵ_1 , ϵ_2 , and M_τ , we can derive a bound on the deviation of the optimal transportation map.

Theorem 4.5. Consider ∇g_0 to be the unbiased ground truth map from Q to P under formulation (4). For $\lambda > 0$ and any other pair (g, f) , where f is α -strongly convex, the following bound holds for solving biased map from formulation (6):

$$\|\nabla g - \nabla g_0\|_{L^2(Q)}^2 \leq \frac{2}{\alpha} (\epsilon_1 + \epsilon_2 + 2\lambda M_\tau).$$

Larger λ would therefore cause the actual-solved map diverging more to the theoretical optimized map. The proof is provided in Appendix A. It builds upon the unbiased formulation bound established by Makkula et al. (2020), with additional consideration for the sparsity gap.

4.1. Dynamic Adjustment to Sparsity Intensity λ

In the previous section, we utilized a constant λ to enforce sparsity in the learned map via ICNN. However, this approach presents inherent challenges: if λ is set too low, the resulting map lacks sufficient sparsity, failing to promote the desired regularization. Conversely, if λ is set too high, the accuracy of the map degrades, leading to a larger deviation of $T_\#(P)$ from the true target Q . This trade-off is clearly illustrated in Figure 2 and additional example Figure 4, where we use the classic eight-Gaussian setup to demonstrate this

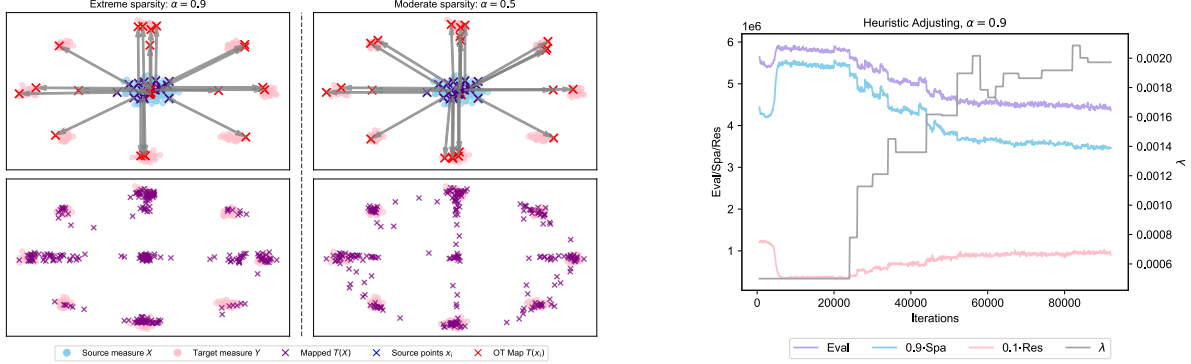


Figure 4. Left: Two classic eight-Gaussian examples are presented, where the source measure is located at the center, and eight target measures are generated from Gaussian distributions. These examples illustrate the trade-off between the sparsity of the map and its feasibility under varying values of α . **Right:** A simulation example demonstrates how λ changes during simulated annealing training under $\alpha = 0.9$, along with the corresponding levels of map sparsity (Spa) and feasibility (Res).

effect. Note that eight-Gaussian example is intended solely for illustrative purposes, as sparsity is not a necessary requirement in this context. In the extreme sparsity case, more and more points collapse towards the source center without adequate transportation to their targets.

We introduce a parameter α to tune this tradeoff by dynamically adjusting λ to optimize a goal function that balances sparsity and feasibility during the ICNN training process. For the map $T_n : X \rightarrow Y$ learned at the n -th iteration of ICNN training, we define its sparsity and feasibility level through two metrics, Spa (Sparsity) and Err (Error), where

$$\text{Spa} = \int_P \tau(T_n(x) - x) dP, \quad \text{Err} = D(T_{n\#}(P), Y).$$

We use the corresponding sparsity metric, τ , during training, while measuring the error through the divergence D between the mapped distribution and the actual target distribution. To capture this geometric divergence, we approximate the source and target distributions, P and Q , as finite sets of sampled points, and use the Wasserstein distance to quantify the divergence between them. However, due to the computational inefficiency of the Wasserstein distance, we accelerate the training process by approximating it with the sliced Wasserstein distance (Bonneel et al., 2015).

It is important to normalize both metrics to the same numerical scale. Ultimately, we construct the evaluation function:

$$\text{Eval} = \alpha \cdot \text{Spa} + (1 - \alpha) \cdot \text{Err}, \quad \alpha \in [0, 1], \quad (8)$$

where α is a pre-determined parameter. A higher value of α leads to a higher sparsity-inducing intensity. The objective is to find the λ that minimizes Eval. Since λ is not explicitly related to Eval, we use the heuristic search by embedding a simulated annealing framework into ICNN, leveraging from its ability to swiftly adapt to adjustments in λ . We heuristically adjust λ after every specific number of iterations (to

give the ICNN sufficient time to smoothly adjust the map with the updated λ). Example of simulation are illustrated in Figure 4, and the algorithm pipeline is shown in Algorithm 1.

Algorithm 1 Heuristic Adjustment Framework for λ

Input: $\alpha, \lambda, n_{\text{ini}}, n_{\text{tr}}, n_{\text{sm}}$; Initial temperature Tem , Min temperature Tem_{min} , Decay rate d

- 1: **Initialize:** Train dual potentials f, g with λ for n_{ini} iterations until stable.
- 2: **while** $Tem > Tem_{\text{min}}$ **do**
- 3: $\lambda \leftarrow \text{SimulatedAnnealing}(Tem, \lambda)$
- 4: map $T_n \leftarrow \text{Train } f, g$ with updated λ for n_{tr} iterations
- 5: $\text{Eval}_n \leftarrow \text{Eval}(T_n)$
- 6: Accept or reject λ based on Eval_n
- 7: **if** Rejected **then**
- 8: Smoothly revert using n_{sm} iterations of training.
- 9: **end if**
- 10: $Tem \leftarrow Tem \cdot d$.
- 11: **end while**

In the simulated annealing framework, we first perform n_{ini} iterations using the starting value of λ to train dual potentials until the map's sparsity and error levels converge to a stable state. After reaching this initial stability, we initiate the simulated annealing process with a starting temperature T . We then continue training dual potentials with the new λ for n_{tr} iterations. To ensure smooth transitioning, if the new λ is not accepted, we perform an additional n_{sm} iterations of training to allow the ICNN to revert smoothly to the previous value of λ .

4.2. High Dimensional Setting

In the high-dimensional setting, a separate framework is required, as it is impractical to impose a sparsity constraint directly on the low dimensional displacement vectors. In-

stead of using the metric to evaluate the map sparsity level, we adopt a more feasible approach by constraining the dimensionality of the displacement vectors in the high-dimensional space. Specifically, given $P, Q \in \mathbb{R}^d$, our goal is to find an optimal transport map T such that all displacement vectors $\Delta(\mathbf{x}) = T(\mathbf{x}) - \mathbf{x}$ lie within a subspace of dimensionality less than l , where $l < d$. Among all maps that satisfy this dimensionality constraint, we aim to find the one that minimizes the divergence between $T_{\#}(P)$ and Q . This optimization problem can be formulated as follows:

$$\begin{aligned} \min_T \quad & \frac{1}{2} \mathbb{E}_{X \sim P} \|T(X) - X\|^2 + \beta D(T_{\#}(P), Q) \\ \text{s.t.} \quad & \dim(T(x_i) - x_i) \leq l, \quad l < d, \quad \forall x_i \in X. \end{aligned}$$

By introducing a divergence regularization term $D(T_{\#}(P), Q)$ with weighting parameter β , we relax the requirement that the source measure P must be exactly transported to the target measure Q (i.e., $T_{\#}(P) = Q$). This formulation is indeed challenging to solve with traditional methods due to the direct constraint on the dimensionality of the vectors. However, our new heuristic framework based on ICNN can efficiently address this problem by doing minor adaptions to Algorithm 1.

Specifically, we can directly apply the smoothed ℓ_0 -norm to regularize the dimensionality of the displacement vectors. Although the smoothed ℓ_0 -norm is not a convex penalty, we empirically observe that increasing λ enhances sparsity, as shown in Figure 5. Therefore, our strategy to adjust λ becomes straightforward: we initially increase λ until the dimensionality requirement is met; then, we decrease λ to minimize $D(T_{\#}(P), Q)$ while maintaining the dimensionality constraint. All the adjustments towards λ are still working on a heuristic framework in Algorithm 1. Detailed pipeline can be found in Appendix B.

5. Experiments

Drug Perturbation & Optimal Transport. Optimal transport has become a powerful tool in cell biology for modeling and predicting cellular responses to drug perturbations (Bunne et al., 2023b). It matches perturbed cells to their original state by measuring high-dimensional features such as single-cell RNA (sc-RNA) expression and 4i (Iterative Indirect Immunofluorescence Imaging) data.

We conducted experiments to evaluate the performance of our sparsity-induced formulation against the original ICNN OT framework and compared it to the Sinkhorn-based sparsity formulation proposed by Cuturi et al. (2023) on two different cell matching tasks.

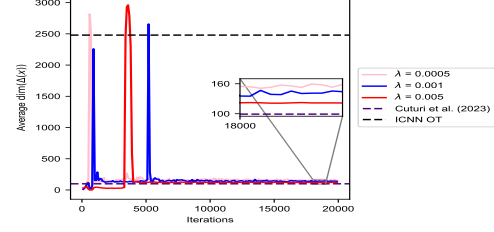


Figure 5. Synthesized sc-RNA perturbation dataset with $n = 4000$ cells, $d = 3000$ genes, and $k = 100$ genes. An OT mapping was learned between the control and treated cells. The average displacement dimensionality during training iterations is shown.

5.1. Synthesized sc-RNA Perturbation Task

Because our first aim was to measure how closely our method could reduce dimensionality to the ground-truth level, we did not run the first task on a real sc-RNA dataset. As real sc-RNA data is unable to allow a reliably accurate determination of the ground truth displacement dimensionality, we built a synthesized dataset for this task, leaving the real dataset for subsequent experiments.

The dataset is constructed as follows: we first define n , the number of cells before and after drug perturbation; d , the total number of genes per cell (overall dimensionality); and k , the number of genes truly affected by the drug (ground-truth dimensionality). Random noise is added to the remaining genes to simulate realistic noise observed in drug perturbation scenarios. The control cells are treated as the source, and the perturbed cells are treated as the target. Using different methods, we compute the OT mapping between two groups of cells. Our objective is to evaluate whether these methods can provide an explainable mapping that focuses exclusively on the truly perturbed genes while disregarding the noisy ones. Example result is shown in Figure 5.

We compare three different methods: ICNN OT, Cuturi et al. (2023)'s approach with the ℓ_1 -norm penalty, and our formulation with the smoothed ℓ_0 -norm penalty under different sparsity-intensity levels (λ). Results in Figure 5 show that, comparing to ICNN OT, our formulation effectively reduces the dimensionality of the displacement map towards the ground-truth level. Cuturi et al. (2023)'s method produces results closest to the ground-truth map. However, neural OT solvers are often preferred in real drug perturbation scenarios because they efficiently handle large, high-dimensional single-cell data, incorporate domain-specific constraints, and are flexible to varying inputs. In contrast, traditional Sinkhorn solvers require storing large cost matrices and multiple iterative updates, making them less scalable.

Table 1. Comparison of different methods' performance.

Method	ICNN OT	Cuturi et al. (2023)	Our Formulation		
			$\lambda = 5 \times 10^{-4}$	$\lambda = 1 \times 10^{-3}$	$\lambda = 5 \times 10^{-3}$
dim($\Delta(\mathbf{x})$)	2480	99	153	138	120

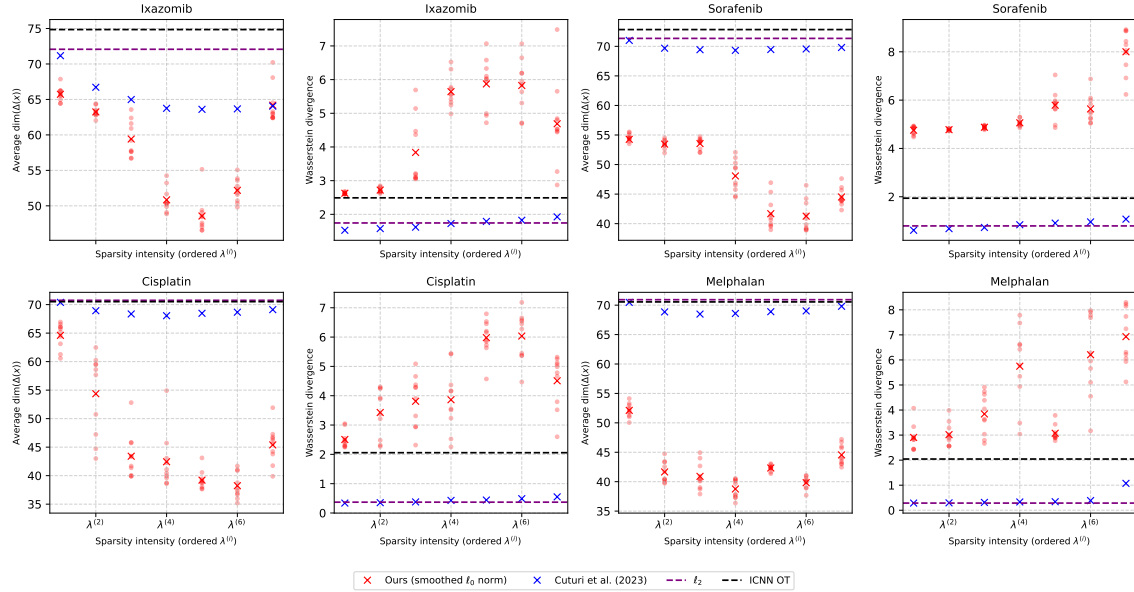


Figure 6. The results of the 4i ($d = 78$ features) perturbation under four different drugs are presented. Each experiment, conducted at a specific λ , displays the average outcome of ten runs. $\lambda^{(i)}$ represents the ordered statistics of each set of λ used in the experiments. Due to the inherent differences in the drugs, $\lambda^{(i)}$ varies across the experiments. $\text{np.isclose}(\cdot, 0)$ is evaluated at the threshold of 10^{-2} to determine the dimensionality of the displacement vectors. Number of cells, n , in each experiment is approximately 12,000 cells.

5.2. Real 4i Perturbation Task

In this section, we use the preprocessed cell 4i perturbation dataset¹, designed for optimal transport matching as utilized in CellOT (Bunne et al., 2023b), to demonstrate the effect of sparsity induction on the displacement vector.

This task assesses the effectiveness of various methods in recovering the OT map, focusing on preserving key features while disregarding less significant ones. Unlike sc-RNA perturbation, where there is a clear separation between noisy and genuinely perturbed cells, recovering the OT map is notably more challenging. Additionally, the absence of a ground-truth map with the true dimensionality further complicates the task. After drug perturbation, the 4i features of the cells are altered, and we use these features to match control cells with perturbed cells. To evaluate the learned map T , we employ two metrics: (i) Average displacement vector dimensionality – *lower values indicate better interpretability*; (ii) Wasserstein divergence between $T_{\#}(P)$ and Q – *lower values indicate better feasibility*.

We selected four drugs (Ixazomib, Sorafenib, Cisplatin, Melphalan) to highlight the improvement of our method towards the existing methods. As shown in Figure 6, among all four drugs, our method could more effectively reduce the dimensionality of the displacement vector. However, several limitations need to be discussed here:

¹Dataset is publicly available at the following site (Bunne et al., 2023a).

Variance of the Results. Due to the inherent randomness in ICNN, the results typically exhibit higher instability as λ increases, leading to more varied outcomes across runs. This aligns with Theorem 4.5, which gives that a larger λ results in a higher error bound. In contrast, the Sinkhorn-based method introduced by Cuturi et al. (2023) consistently achieves convergence in its learned mappings.

Unknown and Varied Minimized Dimensionality. The minimized dimensionality in each experiment varies and is data-driven, making it difficult and impractical to estimate a theoretical or empirical minimum. Therefore, for some dimensionality constraint l from the constrained optimization in §4.2, it may result in no solutions.

Non-convex Penalty under Theoretical Guarantee. Our theoretical guarantee (Theorem 4.3, 4.4) only applies to convex penalties. However, the smoothed ℓ_0 -norm is pseudoconvex and therefore does not benefit from the theoretical guarantee. This can be observed in the dimensionality for the highest λ in each experiment, where the average dimensionality begins to increase. Non-convexity might be a contributing factor, but it is worth noting that the metric used to measure sparsity in Theorem 4.4 is the penalty function τ , whereas we use the direct dimensionality metric in the experiment. All the hyper-parameters setup for each experiments in this work are detailed in Appendix C.

6. Conclusions

We presented a biased, sparsity-inducing formulation based on the unbiased formulation from ICNN OT and demonstrated its reliability in recovering maps with higher displacement sparsity in both low- and high-dimensional experiments. Leveraging ICNN, we also provide a heuristic framework with a flexible objective that can dynamically adjust the sparsity-inducing intensity. Additionally, we adapt this framework to solve the problem with direct constraint on displacement dimensionality in higher-dimensional setting. Several future directions could stem from our work, encompassing both theoretical and empirical aspects. On the theoretical side, these include estimating the theoretical minimized dimension and applying the sparsity-inducing framework to other neural OT solvers (e.g., non-minimax formulations). On the empirical side, directions include studying the effects of hyperparameters and fine-tuning those used in our heuristic framework.

Impact Statement

This paper presents work whose goal is to advance the field of Machine Learning. There are many potential societal consequences of our work, none which we feel must be specifically highlighted here.

Acknowledgement

PC is partially supported by the HKU-IDS Research Grant. YX is supported by Guangdong Province Fundamental and Applied Fundamental Research Regional Joint Fund, (Project 2022B1515130009), and the start-up fund of HKU-IDS. QZ is supported by the National Natural Science Foundation of China (grant no. 71972164) and the Research Grant Council of Hong Kong SAR Government (grant no. 11218221).

This work is supported by computing resources from the HKU-Shanghai ICRC cluster. We would also like to thank Fei Jing from QZ's group for his assistance.

References

Alvarez-Melis, D., Schiff, Y., and Mroueh, Y. Optimizing functionals on the space of probabilities with input convex neural networks. *Transactions on Machine Learning Research*, 2022. ISSN 2835-8856. URL <https://openreview.net/forum?id=dpOYN7o8Jm>.

Amos, B., Xu, L., and Kolter, J. Z. Input convex neural networks. In *Proceedings of the 34th International Conference on Machine Learning*, volume 70 of *Proceedings of Machine Learning Research*, pp. 146–155. PMLR, 2017.

Argyriou, A., Foygel, R., and Srebro, N. Sparse prediction with the k-support norm. In Pereira, F., Burges, C., Bottou, L., and Weinberger, K. (eds.), *Advances in Neural Information Processing Systems*, volume 25. Curran Associates, Inc., 2012. URL https://proceedings.neurips.cc/paper_files/paper/2012/file/99bcfc754a98ce89cb86f73acc04645-Paper.pdf.

Arjovsky, M., Chintala, S., and Bottou, L. Wasserstein generative adversarial networks. In Precup, D. and Teh, Y. W. (eds.), *Proceedings of the 34th International Conference on Machine Learning*, volume 70 of *Proceedings of Machine Learning Research*, pp. 214–223. PMLR, 06–11 Aug 2017. URL <https://proceedings.mlr.press/v70/arjovsky17a.html>.

Asadulaev, A., Korotin, A., Egiazarian, V., Mokrov, P., and Burnaev, E. Neural optimal transport with general cost functionals. In *The Twelfth International Conference on Learning Representations*, 2024. URL <https://openreview.net/forum?id=gIiz7tBtYZ>.

Blondel, M., Seguy, V., and Rolet, A. Smooth and sparse optimal transport. In *Proceedings of the 21st International Conference on Artificial Intelligence and Statistics (AISTATS)*, volume 84 of *Proceedings of Machine Learning Research*, pp. 880–889. PMLR, 2018. URL <http://proceedings.mlr.press/v84/blondel18a/blondel18a.pdf>.

Bonneel, N., Rabin, J., Peyré, G., and Pfister, H. Sliced and radon wasserstein barycenters of measures. *Journal of Mathematical Imaging and Vision*, 51(1):22–45, 2015.

Brenier, Y. Polar factorization and monotone rearrangement of vector-valued functions. *Communications on Pure and Applied Mathematics*, 44(4):375–417, 1991.

Bunne, C., Fatras, K., Flamary, R., Cuturi, M., and Krause, A. Supervised training of conditional monge maps. In Camps-Valls, G., Ruiz, F. J. R., and Valera, I. (eds.), *Proceedings of The 25th International Conference on Artificial Intelligence and Statistics*, volume 151 of *Proceedings of Machine Learning Research*, pp. 1696–1710. PMLR, 2022. URL <https://proceedings.mlr.press/v151/bunne22a.html>.

Bunne, C., Stark, S., Gut, G., Lehmann, K.-V., Pelkmans, L., Krause, R. A., and Rätsch, G. Datasets of learning single-cell perturbation responses using neural optimal transport, 2023a.

Bunne, C., Stark, S. G., Gut, G., et al. Learning single-cell perturbation responses using neural optimal transport. *Nature Methods*, 20:1759–1768, 2023b. doi: 10.1038/s41592-023-01969-x.

Cuturi, M. Sinkhorn distances: Lightspeed computation of optimal transport. In Burges, C., Bottou, L., Welling, M., Ghahramani, Z., and Weinberger, K. (eds.), *Advances in Neural Information Processing Systems*, volume 26. Curran Associates, Inc., 2013. URL https://proceedings.neurips.cc/paper_files/paper/2013/file/af21d0c97db2e27e13572cbf59eb343d-Paper.pdf.

Cuturi, M., Meng-Papaxanthos, L., Tian, Y., Bunne, C., Davis, G., and Teboul, O. Optimal transport tools (ott): A jax toolbox for all things wasserstein. *arXiv preprint arXiv:2201.12324*, 2022.

Cuturi, M., Klein, M., and Ablin, P. Monge, bregman and occam: Interpretable optimal transport in high-dimensions with feature-sparse maps. In *Proceedings of the 40th International Conference on Machine Learning*, volume 202 of *Proceedings of Machine Learning Research*, pp. 6671–6682. PMLR, 2023.

Demetci, P., Santorella, R., Sandstede, B., Noble, W. S., and Singh, R. Scot: single-cell multi-omics alignment with optimal transport. *Journal of Computational Biology*, 29: 3–18, 2022. doi: 10.1089/cmb.2021.0295.

Dunford, N. and Schwartz, J. T. *Linear Operators, Volume 1*. Pure and Applied Mathematics. Wiley-Interscience, New York, 1958. Part 1: General Theory.

Fan, J., Taghvaei, A., and Chen, Y. Scalable computations of wasserstein barycenter via input convex neural networks. In Meila, M. and Zhang, T. (eds.), *Proceedings of the 38th International Conference on Machine Learning*, volume 139 of *Proceedings of Machine Learning Research*, pp. 1571–1581. PMLR, 18–24 Jul 2021. URL <https://proceedings.mlr.press/v139/fan21d.html>.

Gulrajani, I., Ahmed, F., Arjovsky, M., Dumoulin, V., and Courville, A. C. Improved training of Wasserstein GANs. In *Advances in Neural Information Processing Systems*, volume 30, pp. 5767–5777. Curran Associates, Inc., 2017.

Huizing, G.-J., Peyré, G., and Cantini, L. Optimal transport improves cell–cell similarity inference in single-cell omics data. *Bioinformatics*, 38(8):2169–2177, 2022. doi: 10.1093/bioinformatics/btac084. URL <https://doi.org/10.1093/bioinformatics/btac084>.

Klein, M., Pooladian, A.-A., Ablin, P., Ndiaye, E., Niles-Weed, J., and marco cuturi. Learning elastic costs to shape monge displacements. In *The Thirty-eighth Annual Conference on Neural Information Processing Systems*, 2024. URL <https://openreview.net/forum?id=aaUVnpQvbZ>.

Korotin, A., Egiazarian, V., Asadulaev, A., Safin, A., and Burnaev, E. Wasserstein-2 generative networks. In *International Conference on Learning Representations*, 2021a. URL https://openreview.net/forum?id=bEoxzW_Exsa.

Korotin, A., Li, L., Genevay, A., Solomon, J., Filippov, A., and Burnaev, E. Do neural optimal transport solvers work? a continuous wasserstein-2 benchmark. In *Advances in Neural Information Processing Systems*, NIPS ’21. Curran Associates Inc., 2021b.

Liu, T., Puigcerver, J., and Blondel, M. Sparsity-constrained optimal transport. In *Proceedings of the Eleventh International Conference on Learning Representations (ICLR)*, 2023. URL <https://openreview.net/forum?id=yHY9NbQJ5BP>.

Makkuva, A., Taghvaei, A., Oh, S., and Lee, J. Optimal transport mapping via input convex neural networks. In *Proceedings of the 37th International Conference on Machine Learning*, volume 119 of *Proceedings of Machine Learning Research*, pp. 6672–6681. PMLR, 2020.

Mohimani, G. H., Babaie-Zadeh, M., and Jutten, C. Fast sparse representation based on smoothed ℓ_0 norm. In Davies, M. E., James, C. J., Abdallah, S. A., and Plumley, M. D. (eds.), *Independent Component Analysis and Signal Separation*, pp. 389–396, Berlin, Heidelberg, 2007. Springer Berlin Heidelberg.

Mokrov, P., Korotin, A., Li, L., Genevay, A., Solomon, J., and Burnaev, E. Large-scale wasserstein gradient flows. In Beygelzimer, A., Dauphin, Y., Liang, P., and Vaughan, J. W. (eds.), *Advances in Neural Information Processing Systems*, 2021. URL <https://openreview.net/forum?id=nLjIuHsMHp>.

Monge, G. Mémoire sur la théorie des déblais et des remblais. *Histoire de l’Académie Royale des Sciences*, pp. 666–704, 1781.

Rockafellar, R. T. and Wets, R. J.-B. *Variational Analysis*, volume 317 of *Grundlehren der mathematischen Wissenschaften: A Series of Comprehensive Studies in Mathematics*. Springer, Berlin, Heidelberg, 1998. ISBN 978-3-642-64980-6. doi: 10.1007/978-3-642-02431-3.

Schiebinger, G., Shu, J., Tabaka, M., Cleary, B., Subramanian, V., Solomon, A., Gould, J., Liu, S., Lin, S., Berube, P., Lee, L., Chen, J., Brumbaugh, J., Rigollet, P., Hochedlinger, K., Jaenisch, R., Regev, A., and Lander, E. S. Optimal-transport analysis of single-cell gene expression identifies developmental trajectories in reprogramming. *Cell*, 176(4):928–943.e22, 2019. doi: 10.1016/j.cell.2019.01.006.

Schreck, A., Fort, G., Le Corff, S., and Moulines, E. A shrinkage-thresholding metropolis adjusted langevin algorithm for bayesian variable selection. *IEEE Journal of Selected Topics in Signal Processing*, 10(2):366–375, 2015.

Sion, M. On general minimax theorems. *Pacific Journal of Mathematics*, 8(1):171–176, 1958. doi: 10.2140/pjm.1958.8.171.

Taghvaei, A. and Jalali, A. 2-wasserstein approximation via restricted convex potentials with application to improved training for gans, 2019. URL <https://arxiv.org/abs/1902.07197>.

Villani, C. *Topics in Optimal Transportation*, volume 58. American Mathematical Society, 2003.

von Neumann, J. Zur theorie der gesellschaftsspiele. *Mathematische Annalen*, 100:295–320, 1928. doi: 10.1007/BF01448847.

Wang, Y. and Li, J. Improved algorithms for convex-concave minimax optimization. In Larochelle, H., Ranzato, M., Hadsell, R., Balcan, M., and Lin, H. (eds.), *Advances in Neural Information Processing Systems*, volume 33, pp. 4800–4810. Curran Associates, Inc., 2020. URL https://proceedings.neurips.cc/paper_files/paper/2020/file/331316d4efb44682092a006307b9ae3a-Paper.pdf.

Wei, X., Liu, Z., Wang, L., and Gong, B. Improving the improved training of wasserstein GANs. In *International Conference on Learning Representations*, 2018. URL <https://openreview.net/forum?id=SJx9GQb0->.

Zhang, S., Afanassiev, A., Greenstreet, L., Matsumoto, T., and Schiebinger, G. Optimal transport analysis reveals trajectories in steady-state systems. *PLoS Computational Biology*, 17(7):e1009466, 2021. doi: 10.1371/journal.pcbi.1009466.

A. Proofs of Theorems

Proof of Lemma 4.1: Given the assumption on the bounded support of the target measure and the boundedness of ∇g , which is implied by the uniform *Lipschitz* continuity of g in $\mathcal{S}(Q)$ and convexity, we can show that $\tau(\cdot)$ is bounded:

- The smoothed ℓ_0 -norm is bounded because the dimensionality of the target measures is bounded.
- The ℓ_1 -norm is bounded because the magnitude of the displacement vectors is bounded.
- By the Weierstrass theorem, τ_{stvs} is bounded on the compact region covering the value of $\nabla g(y) - y$ since it is continuous.

Given these bounds, we can conclude that Lemma 4.1 holds for all three sparsity penalties used in our analysis.

Theorem A.1 (von Neumann's Minimax Theorem). *Let $X \subset \mathbb{R}^n$ and $Y \subset \mathbb{R}^m$ be two compact and convex sets. Suppose $f : X \times Y \rightarrow \mathbb{R}$ is a continuous function that is concave in x for each fixed y and convex in y for each fixed x (concave-convex). Then, the following equality holds:*

$$\max_{x \in X} \min_{y \in Y} f(x, y) = \min_{y \in Y} \max_{x \in X} f(x, y).$$

Moreover, assuming the optimal solution (x^*, y^*) exists, then it satisfies the following saddle point inequality:

$$f(x, y^*) \leq f(x^*, y^*) \leq f(x^*, y), \quad \forall x \in X, y \in Y,$$

In the context of ICNN, our sets X and Y are instead topological vector spaces, which places them under the scope of a variant of von Neumann's Minimax Theorem: Sion's Minimax Theorem (Sion, 1958).

Lemma A.2. *For equation (4), given $f \in \text{CVX}(P)$ and $g \in \text{CVX}(Q)$, the function*

$$\mathcal{V}_{P,Q}(f, g) = -\mathbb{E}_P[f(X)] - \mathbb{E}_Q[\langle Y, \nabla g(Y) \rangle - f(\nabla g(Y))]$$

is a concave-convex and continuous function.

Proof of Lemma A.2 — Concave-Convex: To prove that $\mathcal{V}_{P,Q}(f, g)$ is a concave-convex function, we first show that, for a fixed g , $\mathcal{V}_{P,Q}(f, g)$ is concave in f .

Consider any two functions $f_1, f_2 \in \text{CVX}(P)$ and any $\alpha \in [0, 1]$. We aim to show that:

$$\mathcal{V}_{P,Q}(\alpha f_1 + (1 - \alpha) f_2, g) \geq \alpha \mathcal{V}_{P,Q}(f_1, g) + (1 - \alpha) \mathcal{V}_{P,Q}(f_2, g). \quad (9)$$

To demonstrate this, note that by linearity:

$$\begin{aligned} \mathcal{V}_{P,Q}(\alpha f_1 + (1 - \alpha) f_2, g) &= -\mathbb{E}_P[(\alpha f_1 + (1 - \alpha) f_2)(X)] \\ &\quad - \mathbb{E}_Q[\langle Y, \nabla g(Y) \rangle - (\alpha f_1 + (1 - \alpha) f_2)(\nabla g(Y))] \\ &= -\alpha \mathbb{E}_P[f_1(X)] - (1 - \alpha) \mathbb{E}_P[f_2(X)] \\ &\quad + \alpha \mathbb{E}_Q[f_1(\nabla g(Y))] + (1 - \alpha) \mathbb{E}_Q[f_2(\nabla g(Y))] \\ &\quad - \mathbb{E}_Q[\langle Y, \nabla g(Y) \rangle] \\ &= \alpha \mathcal{V}_{P,Q}(f_1, g) + (1 - \alpha) \mathcal{V}_{P,Q}(f_2, g). \end{aligned}$$

This establishes that $\mathcal{V}_{P,Q}(f, g)$ is concave in f for a fixed g .

Next, we show that for a fixed f , $\mathcal{V}_{P,Q}(f, g)$ is convex in g . Consider any $g_1, g_2 \in \text{CVX}(Q)$ and any $\alpha \in [0, 1]$. We need to prove that:

$$\mathcal{V}_{P,Q}(f, \alpha g_1 + (1 - \alpha) g_2) \leq \alpha \mathcal{V}_{P,Q}(f, g_1) + (1 - \alpha) \mathcal{V}_{P,Q}(f, g_2). \quad (10)$$

By definition, we have:

$$\begin{aligned}
 \mathcal{V}_{P,Q}(f, \alpha g_1 + (1 - \alpha)g_2) &= -\mathbb{E}_P[f(X)] \\
 &\quad - \mathbb{E}_Q[\langle Y, \alpha \nabla g_1(Y) + (1 - \alpha) \nabla g_2(Y) \rangle - f(\alpha \nabla g_1(Y) + (1 - \alpha) \nabla g_2(Y))] \\
 &= -\mathbb{E}_P[f(X)] - \mathbb{E}_Q[\langle Y, \alpha \nabla g_1(Y) \rangle + \langle Y, (1 - \alpha) \nabla g_2(Y) \rangle] \\
 &\quad + \mathbb{E}_Q[f(\alpha \nabla g_1(Y) + (1 - \alpha) \nabla g_2(Y))] \\
 &\leq -\mathbb{E}_P[f(X)] - \mathbb{E}_Q[\langle Y, \alpha \nabla g_1(Y) \rangle + \langle Y, (1 - \alpha) \nabla g_2(Y) \rangle] \\
 &\quad + \mathbb{E}_Q[\alpha f(\nabla g_1(Y)) + (1 - \alpha) f(\nabla g_2(Y))] \quad (\because f \text{ is convex}).
 \end{aligned}$$

Combining the terms, we obtain the desired inequality (10). Therefore, by combining inequalities (9) and (10), we conclude that $\mathcal{V}_{P,Q}(f, g)$ is indeed a concave-convex function. \square

Proof of Lemma A.2 — Continuity: We aim to prove that $\mathcal{V}_{P,Q}(f, g)$ is continuous under the assumptions: **(i)** Q has bounded support; **(ii)** Every g in $\mathcal{S}(Q)$ is L -Lipschitz, which means $\|\nabla g(\cdot)\| \leq L$. We assume that $\nabla g(\cdot)$ is L -Lipschitz; **(iii)** Every f in $\mathcal{S}(P)$ is also L -Lipschitz; **(iv)** We assume $\mathcal{S}(P)$ and $\mathcal{S}(Q)$ under the uniform convergence topology, i.e., $(f_n, g_n) \rightarrow (f, g)$ means $f_n \rightarrow f$ uniformly and $g_n \rightarrow g$ uniformly on their respective domains. Moreover, given f and g is L -Lipschitz and convex, it's sufficient to show that $(f_n, g_n) \rightarrow (f, g)$ is also under epi-convergence.

By Rockafellar & Wets (1998, Theorem 12.35), if g_n are convex and epi-convergent to a convex g , then under suitable regularity conditions (each g_n being differentiable on a compact domain, with uniformly bounded gradients), we get $\nabla g_n(y) \rightarrow \nabla g(y)$ pointwise in y .

Since each g_n is L -Lipschitz on a compact domain, it follows that $\|\nabla g_n(\cdot)\| \leq L$. Moreover, the family $\{\nabla g_n\}$ is equicontinuous:

$$\|\nabla g_n(x) - \nabla g_n(y)\| \leq \|\nabla g_n(x)\| + \|\nabla g_n(y)\| \leq 2L$$

Under Arzelà–Ascoli Theorem, for a compact set, equicontinuity plus pointwise convergence imply $\nabla g_n \rightarrow \nabla g$ uniformly. Therefore, we have

$$\nabla g_n(y) \rightarrow \nabla g(y) \quad \text{uniformly for } y \in \text{supp}(Q).$$

Since each f_n is also L -Lipschitz, we have uniform continuity on any bounded set. Because $\|\nabla g_n(y)\| \leq L$, $\nabla g_n(y)$ indeed lies in the ball of radius L , which we denote this ball by $\mathcal{B}_L(0)$.

For y in the bounded support of Q , we then examine

$$|f_n(\nabla g_n(y)) - f(\nabla g(y))| \leq \underbrace{|f_n(\nabla g_n(y)) - f(\nabla g_n(y))|}_{(I)} + \underbrace{|f(\nabla g_n(y)) - f(\nabla g(y))|}_{(II)}.$$

For part (I), since $f_n \rightarrow f$ in uniform convergence and bounded by uniform norm, we get

$$\sup_{\|z\| \leq L} |f_n(z) - f(z)| \xrightarrow{n \rightarrow \infty} 0.$$

Therefore, $|f_n(\nabla g_n(y)) - f(\nabla g_n(y))| \rightarrow 0$ uniformly in y .

For part (II), because f is L -Lipschitz, it's then uniformly continuous on the ball $\mathcal{B}_L(0)$. Hence if $\|\nabla g_n(y) - \nabla g(y)\| \leq \delta$, then we have

$$|f(\nabla g_n(y)) - f(\nabla g(y))| < \varepsilon(\delta),$$

where $\varepsilon(\delta) \rightarrow 0$ as $\delta \rightarrow 0$. Since $\nabla g_n \rightarrow \nabla g$ uniformly, $\|\nabla g_n(y) - \nabla g(y)\|$ can be made small independently of y .

Integrating (I) and (II) together, we can conclude

$$f_n(\nabla g_n(y)) \rightarrow f(\nabla g(y)) \quad \text{uniformly in } y \in \text{supp}(Q).$$

After studying the behavior of $f_n(\nabla g_n(y))$, we finally move the whole part of $\mathcal{V}_{p,q}(f, g)$; we first define

$$\mathcal{V}_{P,Q}(f_n, g_n) = -\mathbb{E}_P[f_n(X)] - \mathbb{E}_Q[\langle Y, \nabla g_n(Y) \rangle - f_n(\nabla g_n(Y))].$$

We then compare $\mathcal{V}_{P,Q}(f_n, g_n)$ and $\mathcal{V}_{P,Q}(f, g)$ part by part:

$$|\mathcal{V}_{P,Q}(f_n, g_n) - \mathcal{V}_{P,Q}(f, g)| \leq \underbrace{|\mathbb{E}_P[f_n(X)] - \mathbb{E}_P[f(X)]|}_{(I)} + \underbrace{|\mathbb{E}_Q[\langle Y, \nabla g_n(Y) \rangle - f_n(\nabla g_n(Y))] - \mathbb{E}_Q[\langle Y, \nabla g(Y) \rangle - f(\nabla g(Y))]|}_{(II)}.$$

For part (I), since X lies in the bounded support of $\mathcal{S}(P)$ and $f_n \rightarrow f$ uniformly, we have $f_n(X) \rightarrow f(X)$ for all X . Uniform convergence on a bounded support measure implies $\mathbb{E}_P[f_n(X)] \rightarrow \mathbb{E}_P[f(X)]$.

For part (II), we have already showed that $\nabla g_n(Y) \rightarrow \nabla g(Y)$ and $f_n(\nabla g_n(Y)) \rightarrow f(\nabla g(Y))$ uniformly in Y . Also, $\langle Y, \nabla g_n(Y) \rangle \rightarrow \langle Y, \nabla g(Y) \rangle$ uniformly because Y lies in a bounded set and $\nabla g_n(Y)$ is uniformly bounded and convergent to $\nabla g(Y)$. Therefore, $[\langle Y, \nabla g_n(Y) \rangle - f_n(\nabla g_n(Y))]$ converges uniformly to $[\langle Y, \nabla g(Y) \rangle - f(\nabla g(Y))]$. Since Q is a probability measure on a bounded domain and the integrand is uniformly bounded (by a constant depending on L and the radius of $\mathcal{S}(Q)$), we can again use standard dominated-convergence arguments to conclude

$$\mathbb{E}_Q[\langle Y, \nabla g_n(Y) \rangle - f_n(\nabla g_n(Y))] \rightarrow \mathbb{E}_Q[\langle Y, \nabla g(Y) \rangle - f(\nabla g(Y))].$$

Combining (a) and (b), we see that

$$\lim_{n \rightarrow \infty} |\mathcal{V}_{P,Q}(f_n, g_n) - \mathcal{V}_{P,Q}(f, g)| = 0,$$

which shows

$$\mathcal{V}_{P,Q}(f_n, g_n) \rightarrow \mathcal{V}_{P,Q}(f, g).$$

Therefore, $\mathcal{V}_{P,Q}$ is continuous with respect to (f, g) in the uniform convergence topology under the stated assumptions.

With Lemma 4.1, Theorem A.1, and Lemma A.2, we can then prove Theorem 4.2. \square

Proof of Theorem 4.2: As defined in §4, let $s(g) = \int_{\mathbb{R}^d} \tau(\nabla g(y) - y) dQ$. We first aim to prove that $J_\lambda \geq J_0$. This follows from the non-negativity of $\tau(\cdot)$ and λ , which implies:

$$\mathcal{V}_{P,Q}(f, g) + \lambda s(g) \geq \mathcal{V}_{P,Q}(f, g).$$

Taking the infimum over g on both sides and then the supremum over f , we obtain:

$$\sup_{f \in \text{ICNN}(\mathbb{R}^d)} \inf_{g \in \text{ICNN}(\mathbb{R}^d)} (\mathcal{V}_{P,Q}(f, g) + \lambda s(g)) \geq \sup_{f \in \text{ICNN}(\mathbb{R}^d)} \inf_{g \in \text{ICNN}(\mathbb{R}^d)} \mathcal{V}_{P,Q}(f, g),$$

which is equivalent to the inequality $J_\lambda \geq J_0$. To show that $\lim_{\lambda \rightarrow 0} J_\lambda = J_0$, it remains to prove that $\lim_{\lambda \rightarrow 0} J_\lambda \leq J_0$.

Let (f_0, g_0) be the optimal solution corresponding to J_0 . Since f and g are parameterized from a convex space and $\mathcal{V}_{P,Q}(f, g)$ is a concave-convex function (as established in Lemma A.3), by Theorem A.1, we have:

$$\mathcal{V}_{P,Q}(f, g_0) \leq \mathcal{V}_{P,Q}(f_0, g_0) = J_0. \quad (11)$$

Now, consider the compactness of the function space $\text{ICNN}(\mathbb{R}^d)$, there exists $(\widetilde{f}_\lambda, \widetilde{g}_\lambda)$ that is the optimal solution corresponding to J_λ . For this supremum-infimum formulation, we have:

$$J_\lambda = \mathcal{V}_{P,Q}(f_\lambda, g_\lambda) + \lambda s(g_\lambda) \leq \mathcal{V}_{P,Q}(f_\lambda, g) + \lambda s(g). \quad (12)$$

Note that Theorem A.1 does not necessarily apply to J_λ , since $\tau(\cdot)$ may not be convex, so only one side of the saddle point inequality holds. Substituting $g = g_0$ into (12), we obtain:

$$J_\lambda \leq \mathcal{V}_{P,Q}(f_\lambda, g_0) + \lambda s(g_0).$$

Taking the upper limit as $\lambda \rightarrow 0$, we have:

$$\limsup_{\lambda \rightarrow 0} J_\lambda \leq \limsup_{\lambda \rightarrow 0} [\mathcal{V}_{P,Q}(f_\lambda, g_0) + \lambda s(g_0)].$$

By Lemma 4.1, since $S(g)$ is bounded, $\lim_{\lambda \rightarrow 0} \lambda S(g) = 0$, so:

$$\limsup_{\lambda \rightarrow 0} J_\lambda \leq \mathcal{V}_{P,Q}(f_\lambda, g_0). \quad (13)$$

Substituting $f = f_\lambda$ into (11), we have:

$$\mathcal{V}_{P,Q}(f_\lambda, g_0) \leq \mathcal{V}_{P,Q}(f_0, g_0) = J_0. \quad (14)$$

Combining (13) and (14), we obtain:

$$\limsup_{\lambda \rightarrow 0} J_\lambda \leq \mathcal{V}_{P,Q}(f_\lambda, g_0) \leq \mathcal{V}_{P,Q}(f_0, g_0) = J_0.$$

Thus, with $J_\lambda \geq J_0$ and $\limsup_{\lambda \rightarrow 0} J_\lambda \leq J_0$, Theorem 4.2 is proved. \square

Proof of Theorem 4.3: After proving Theorem 4.2, we aim to show that when $\lambda \rightarrow 0$,

$$\text{dist}\left((g_\lambda, f_\lambda), \mathcal{G}\right) \rightarrow 0,$$

Under Assumption 3.1, the sets $\mathcal{S}(P)$ and $\mathcal{S}(Q)$ are uniformly compact and uniformly bounded in L^∞ , with their essential supremum providing the uniform bound. Additionally, by Lemma 4.1, all $f \in \mathcal{S}(P)$ and $g \in \mathcal{S}(Q)$ are L -Lipschitz continuous, which implies that $\mathcal{S}(P)$ and $\mathcal{S}(Q)$ are *equicontinuous*.

The combination of uniform boundedness in L^∞ and *equicontinuity* implies that $\mathcal{S}(P)$ and $\mathcal{S}(Q)$ satisfy the conditions of the Arzelà-Ascoli Theorem. Applying the theorem on arbitrary compact metric spaces, or more generally, on compact Hausdorff spaces, ensures the existence of a convergent subsequence.

Consider a sequence of optimal solutions $(f_{\lambda_n}, g_{\lambda_n}) \in \mathcal{S}(P) \times \mathcal{S}(Q)$ corresponding to a sequence $\lambda_n \rightarrow 0$. Due to the compactness of $\mathcal{S}(P) \times \mathcal{S}(Q)$, there exists a uniformly convergent subsequence $(f_{\lambda_{n_k}}, g_{\lambda_{n_k}}) \rightarrow (f', g')$, where $(f', g') \in \mathcal{S}(P) \times \mathcal{S}(Q)$.

This result relies on the fact that the uniform boundedness in L^∞ ensures the subsequential limits retain their essential supremum bounds, and the equicontinuity guarantees convergence in the uniform topology. The completeness of L^∞ further ensures the limit functions f' and g' are well-defined within $\mathcal{S}(P)$ and $\mathcal{S}(Q)$, respectively, which validates the application of the Arzelà-Ascoli Theorem in this context (Dunford & Schwartz, 1958).

Since $\lim_{\lambda \rightarrow 0} J_\lambda = J_0$, we have:

$$\lim_{n \rightarrow \infty} J_{\lambda_n} = J_0.$$

Consequently,

$$\lim_{n \rightarrow \infty} J_{\lambda_n} = \lim_{n \rightarrow \infty} \mathcal{V}_{P,Q}(f_{\lambda_n}, g_{\lambda_n}) + \lambda_n s(g_{\lambda_n}) = \mathcal{V}_{P,Q}(f', g').$$

This implies that:

$$\mathcal{V}_{P,Q}(f', g') = J_0 = \mathcal{V}_{P,Q}(f_0, g_0).$$

Since $\mathcal{V}_{P,Q}(f, g) + \lambda s(g)$ is concave-convex when $\tau(\cdot)$ is convex, saddle point inequality holds for both J_λ and J_0 . Note that such saddle point is unique given the objective function is strongly concave-strongly convex (Wang & Li, 2020). Our objective function is only concave-convex, which indicates that the convergent subsequence would possibly converge to a set of saddle points \mathcal{G} .

Due to the continuity of $\mathcal{V}_{P,Q}(f, g)$, the set \mathcal{G} is closed. Therefore, we conclude that:

$$\lim_{\lambda \rightarrow 0} \text{dist}\left((g_\lambda, f_\lambda), \mathcal{G}\right) = 0,$$

It is important to note that when $\tau(\cdot)$ is non-convex, while a convergent subsequence may still exist, the convergence to (f_0, g_0) is not guaranteed to hold. \square

Proof of Theorem 4.4: We first define:

$$J_{\lambda_1} = C_{P,Q} + \sup_{f \in \text{ICNN}(\mathbb{R}^d)} \inf_{g \in \text{ICNN}(\mathbb{R}^d)} \mathcal{V}_{P,Q}(f, g) + \lambda_1 s(g),$$

$$J_{\lambda_2} = C_{P,Q} + \sup_{f \in \text{ICNN}(\mathbb{R}^d)} \inf_{g \in \text{ICNN}(\mathbb{R}^d)} \mathcal{V}_{P,Q}(f, g) + \lambda_2 s(g).$$

Consider $(f_{\lambda_1}, g_{\lambda_1})$ and $(f_{\lambda_2}, g_{\lambda_2})$ be the optimal solution to respect J_{λ_1} and J_{λ_2} , we aim to prove that given $\lambda_1 < \lambda_2$, we have

$$s(g_{\lambda_1}) \geq s(g_{\lambda_2}).$$

By the saddle point inequality, we have the following four inequalities,

$$\mathcal{V}_{P,Q}(f_{\lambda_1}, g_{\lambda_1}) + \lambda_1 s(g_{\lambda_1}) \leq \mathcal{V}_{P,Q}(f_{\lambda_1}, g_{\lambda_2}) + \lambda_1 s(g_{\lambda_2}), \quad (15)$$

$$\mathcal{V}_{P,Q}(f_{\lambda_2}, g_{\lambda_2}) + \lambda_2 s(g_{\lambda_2}) \leq \mathcal{V}_{P,Q}(f_{\lambda_2}, g_{\lambda_1}) + \lambda_2 s(g_{\lambda_1}), \quad (16)$$

$$\mathcal{V}_{P,Q}(f_{\lambda_1}, g_{\lambda_1}) + \lambda_1 s(g_{\lambda_1}) \geq \mathcal{V}_{P,Q}(f_{\lambda_2}, g_{\lambda_1}) + \lambda_1 s(g_{\lambda_1}), \quad (17)$$

$$\mathcal{V}_{P,Q}(f_{\lambda_2}, g_{\lambda_2}) + \lambda_2 s(g_{\lambda_2}) \geq \mathcal{V}_{P,Q}(f_{\lambda_1}, g_{\lambda_2}) + \lambda_2 s(g_{\lambda_2}). \quad (18)$$

By (17) and (18), we have

$$\mathcal{V}_{P,Q}(f_{\lambda_1}, g_{\lambda_1}) \geq \mathcal{V}_{P,Q}(f_{\lambda_2}, g_{\lambda_1}), \quad (19)$$

$$\mathcal{V}_{P,Q}(f_{\lambda_2}, g_{\lambda_2}) \geq \mathcal{V}_{P,Q}(f_{\lambda_1}, g_{\lambda_2}). \quad (20)$$

Rearranging (15) and (16), we have

$$\mathcal{V}_{P,Q}(f_{\lambda_1}, g_{\lambda_1}) - \mathcal{V}_{P,Q}(f_{\lambda_1}, g_{\lambda_2}) + \mathcal{V}_{P,Q}(f_{\lambda_2}, g_{\lambda_2}) - \mathcal{V}_{P,Q}(f_{\lambda_2}, g_{\lambda_1}) \leq (\lambda_1 - \lambda_2)[s(g_{\lambda_2}) - s(g_{\lambda_1})].$$

With (19) and (20), we can get

$$\begin{aligned} 0 &\leq (\lambda_1 - \lambda_2)[s(g_{\lambda_2}) - s(g_{\lambda_1})], \\ s(g_{\lambda_1}) &\geq s(g_{\lambda_2}) \quad (\because \lambda_1 < \lambda_2). \end{aligned}$$

□

Proof of Theorem 4.5: We first define the optimality gaps $\hat{\epsilon}_1$ and $\hat{\epsilon}_2$ for unbiased formulation (4)

$$\hat{\epsilon}_1(f, g) = \mathcal{V}_{P,Q}(f, g) - \inf_{g' \in \mathcal{S}(Q)} \mathcal{V}_{P,Q}(f, g'),$$

$$\hat{\epsilon}_2(f) = \mathcal{V}_{P,Q}(f_0, g_0) - \inf_{g' \in \mathcal{S}(Q)} \mathcal{V}_{P,Q}(f, g').$$

Leveraging from Theorem 3.6 from [Makkluva et al. \(2020\)](#), we then aim to bound $\{\hat{\epsilon}_1, \hat{\epsilon}_2\}$ using $\{\epsilon_1, \epsilon_2\}$ and therefore bounding the upper bound of the map error:

$$\begin{aligned} \hat{\epsilon}_1(f, g) &= \mathcal{V}_{P,Q}(f, g) - \inf_{g' \in \mathcal{S}(Q)} \mathcal{V}_{P,Q}(f, g') \\ &\leq [\mathcal{V}_{P,Q}(f, g) + \lambda s(g)] - [\mathcal{V}_{P,Q}(f, f^*) + \lambda s(f^*)] + \lambda s(f^*) \\ &\leq \mathcal{N}_{P,Q}(f, g) - \inf_{g' \in \mathcal{S}(Q)} \mathcal{N}_{P,Q}(f, g') + \lambda s(f^*) \\ &\leq \epsilon_1(f, g) + \lambda M_\tau \end{aligned}$$

Similarly,

$$\begin{aligned} \hat{\epsilon}_2(f) &= \mathcal{V}_{P,Q}(f_0, g_0) - \inf_{g' \in \mathcal{S}(Q)} \mathcal{V}_{P,Q}(f, g') \\ &\leq \mathcal{V}_{P,Q}(f_\lambda, g_\lambda) - \inf_{g' \in \mathcal{S}(Q)} \mathcal{V}_{P,Q}(f, g') \\ &\leq [\mathcal{V}_{P,Q}(f_\lambda, g_\lambda) + \lambda s(g_\lambda)] - [\lambda s(g') - \inf_{g' \in \mathcal{S}(Q)} \mathcal{V}_{P,Q}(f, g')] + \lambda s(g') \\ &\leq [\mathcal{V}_{P,Q}(f_\lambda, g_\lambda) + \lambda s(g_\lambda)] - \inf_{\tilde{g} \in \mathcal{S}(Q)} \mathcal{N}_{P,Q}(f, \tilde{g}) + \lambda s(g') \\ &\leq \epsilon_2(f) + \lambda M_\tau \end{aligned}$$

By Theorem 3.6 from [Makkuva et al. \(2020\)](#), we therefore have

$$\|\nabla g - \nabla g_0\|_{L^2(Q)}^2 \leq \frac{2}{\alpha} (\hat{\epsilon}_1 + \hat{\epsilon}_2) \leq \frac{2}{\alpha} (\epsilon_1 + \epsilon_2 + 2\lambda M_\tau).$$

B. Adapted Heuristic Adjustment Algorithm for High Dimensional Setting

Our method is straightforward: we first increase λ to ensure that the displacement vectors meet the dimensionality constraint. Then, we heuristically decrease λ to reduce the intensity of sparsity-inducing, allowing the model to learn a more feasible map. The details of this algorithm are illustrated in Algorithm 2.

Algorithm 2 Heuristic Framework for High-Dimensional Setting

Input: Initialization iterations n_{ini} , Training iterations n_{tr} , Smoothing iterations n_{sm}

Initial temperature T , Minimum temperature T_{min} , Decay rate d

Initial intensity λ , Intensity growth rate ir , Dimension threshold l

- 1: **Initialize:** Train dual potentials f, g with λ for n_{ini} iterations.
- 2: Compute dimensionality of displacement vectors: $\text{Dim} \leftarrow \text{Dim}(\text{Map})$.
- 3: **while** $\text{Dim} \geq l$ **do**
- 4: Increase sparsity intensity: $\lambda \leftarrow \lambda \cdot (1 + ir)$.
- 5: Train f, g with updated λ for n_{tr} iterations.
- 6: Update dimensionality: $\text{Dim} \leftarrow \text{Dim}(\text{Map})$.
- 7: **end while**
- 8: **while** $T > T_{\text{min}}$ **do**
- 9: Adjust λ within range: $\lambda_{\text{new}} \leftarrow \lambda \cdot (1 + \text{random}(-\text{Range}, 0))$.
- 10: Train f, g with λ_{new} for n_{tr} iterations.
- 11: Update dimensionality: $\text{Dim}_{\text{new}} \leftarrow \text{Dim}(\text{Map})$.
- 12: **if** $\text{Dim}_{\text{new}} \geq l$ **then**
- 13: Accept new λ : $\lambda \leftarrow \lambda_{\text{new}}$.
- 14: **end if**
- 15: Smoothly adjust with n_{sm} iterations if needed.
- 16: Update temperature: $T \leftarrow T \cdot d$.
- 17: **end while**

C. Hyper-parameter Setup

Hyperparameters for Figure 4. We use most of the default hyperparameters for ICNN training. For iteration-related hyperparameters, we set $n_{\text{ini}} = 20,000$ and $n_{\text{tr}} = n_{\text{sm}} = 2,000$. For simulated annealing hyperparameters, we set the initial temperature to 1.0, the minimum temperature to 0.15, the temperature decay rate to 0.95, and the range adjustment parameter $p = 3$. For the τ_{stvs} penalty, we set $\gamma = 100$.

Hyperparameters for Figure 5. For the ICNN OT results, we largely use the default hyperparameter settings outlined in the original paper, with a modification to the batch size, which is set to 128 to better accommodate our datasets. For our results, we also use the same set of default parameters as ICNN OT. The parameter for the smoothed ℓ_0 -norm is set to $\sigma = 1.0$. For the results from [Cuturi et al. \(2023\)](#), we set the entropic regularization to $\epsilon = 10^{-3}$ and the sparsity regularization intensity to $\lambda = 2$.

Hyperparameters for Figure 6. The default training parameters for ICNN are used here as well. We primarily experiment with different sparsity regularization intensities λ . For all four drugs, we use the same set of parameters $\lambda^{(i)} = [0.01, 0.1, 0.2, 0.5, 0.8, 1, 2]$ for the results from [Cuturi et al. \(2023\)](#), as the outcomes do not vary significantly across experiments. The dimensionality, however, starts to increase as λ approaches 1. For our results, we find that each experiment varies under different parameter settings. Therefore, we adjust the parameters for each experiment to better illustrate how the dimensionality changes with different intensities.

- For Ixazomib, we use $\lambda^{(i)} = [0.0001, 0.0005, 0.001, 0.0015, 0.002, 0.0025, 0.005]$.
- For Sorafenib, we use $\lambda^{(i)} = [0.001, 0.0015, 0.002, 0.0025, 0.003, 0.004, 0.005]$.

- For Cisplatin, we use $\lambda^{(i)} = [0.0001, 0.0005, 0.001, 0.0015, 0.0025, 0.004, 0.005]$.
- For Melphalan, we use $\lambda^{(i)} = [0.0002, 0.0005, 0.002, 0.0025, 0.0035, 0.004, 0.005]$.